LI, Y., REN, J., GAO, Z. and SUN, G. 2024. Sparse autoencoder based hyperspectral anomaly detection with the singular spectrum analysis based spectral denoising. In *Proceedings of the 2024 IEEE International geoscience and remote sensing symposium (IGARSS 2024), Athens, Greece, 7-12 July 2024*. Piscataway: IEEE [online], pages 9210-9213. Available from: https://doi.org/10.1109/igarss53475.2024.10641314

Sparse autoencoder based hyperspectral anomaly detection with the singular spectrum analysis based spectral denoising.

LI, Y., REN, J., GAO, Z. and SUN, G.

2024

© 2024 IEEE. Personal use of this material is permitted. Permission from IEEE must be obtained for all other uses, in any current or future media, including reprinting/republishing this material for advertising or promotional purposes, creating new collective works, for resale or redistribution to servers or lists, or reuse of any copyrighted component of this work in other works.

OpenAIR @RGU

This document was downloaded from https://openair.rgu.ac.uk

CC BY

SPARSE AUTOENCODER BASED HYPERSPECTRAL ANOMALY DETECTION WITH THE SINGULAR SPECTRUM ANALYSIS BASED SPECTRAL DENOISING

Yinhe Li[1], Jinchang Ren[1], Zhi Gao[2], Genyun Sun[3]

[1] National Subsea Centre, Robert Gordon University, Aberdeen, U.K.
[2] School of Remote Sensing and Information Engineering, Wuhan University, Wuhan, China
[3] College of Oceanography and Space Informatics, China University of Petroleum (East China), Qingdao, China.

ABSTRACT

As an effective tool for monitoring surface irregularities in remote sensing, hyperspectral anomaly detection (HAD) has garnered increasing attention. However, how to improve the detection accuracy remains a formidable challenge, due mainly to the noise and variations in the spectral domain, especially when there is lack of the labelled data for training. To tackle these difficulties, a novel unsupervised HAD method is proposed. First, 1-D Singular Spectrum Analysis (SSA) is employed to eliminate outliers in the spectral domain. Second, the SSA-smoothed hypercube undergoes a sparse autoencoder for background reconstruction, where the reconstruction error is used to extract anomalous pixels. Finally, the RX algorithm is employed to segment anomalous pixels from the background. Comprehensive experiments on four publicly available datasets have validated the superior performance of our method in effectively enhancing the separability between anomaly pixels and their respective backgrounds, outperforming a few state-of-the-art methods, particularly in terms of the detection accuracy.

Index Terms— Hyperspectral images, anomaly detection, singular spectrum analysis, sparse autoencoder, RX.

1. INTRODUCTION

Hyperspectral remote sensing (HRS) has emerged as a transformative technology in Earth observation, thanks to the combined spectral and spatial information it contains [1]. As one of the most important research topics and application areas in HRS, hyperspectral anomaly detection (HAD) has grabbed increasing attention. As the anomaly features are different from the background, they can be potentially identified even through unsupervised algorithms based on statistics or feature extraction without the need for prior information [2]. As a result, HAD has been widely applied in numerous areas, especially in military and civilian fields.

In recent years, many HAD methods have been proposed. One classic algorithm is the Reed-Xiaoli (RX) method [3], which operates under the assumption that the background in a Hyperspectral Image (HSI) follows a Gaussian multivariate distribution, represented using the mean vector and the covariance matrix. The Mahalanobis distance is employed to calculate the anomaly value between each pixel and the background. Inspired by the RX algorithm, several variations have also been developed, such as the kernel RX [4] and the local RX [5] algorithms, aiming to enhance the performance and adaptability of the original RX for anomaly detection in HSI. Nevertheless, employing the RX algorithm directly comes with certain drawbacks, especially the sensitivity to the spectral noise, which exists widely in the spectral data.

Another classic algorithm is based on the representation models, which operate under the assumption that background pixels can be precisely represented using correlated samples. In contrast, anomalies cannot be effectively represented in the same manner. The most representative method here is the collaborative representation detection [6]. With a dual-window strategy, it operates under the assumption that background samples can be effectively represented by the surrounding pixels, while anomalies cannot.

Besides, some advanced representation-based methods have been proposed to improve the HAD accuracy, such as the low-rank and sparse representation (LRASR) [7], low-rank and sparse matrix decomposition-based Mahalanobis distance method (LSMAD) [8], visual attention model and background subtraction with adaptive weight (VABS) [9]. However, these methods also have drawbacks, especially in determining the regularization parameters due to the lack of prior knowledge about the anomalies. In addition, image priors are frequently suboptimal when applied to real data.

The autoencoder (AE)-based method capitalizes on the assumption that the background constitutes a significant proportion, while the anomaly occupies a smaller portion. This approach effectively reconstructs the background and inadequately reconstructs the anomaly, utilizing the reconstruction error to calculate anomaly values. Drawing inspiration from this concept, in this study, we propose an unsupervised algorithm based on the sparse AE on the SSA smoothed his, as detailed below.

2. PROPSED METHOD

The flowchart of the proposed algorithm is illustrated in Fig. 1, containing three main parts. Initially, we employ the

first component of SSA to derive the smoothed hypercube so as to mitigate the noise and outliers in the spectral domain. The denoised hypercube is subsequently fed into a sparse AE model for background reconstruction. We extract anomalous targets based on the reconstruction error. Ultimately, the conventional RX algorithm is used to segment the anomalous pixels from the background. These are detailed as follows.

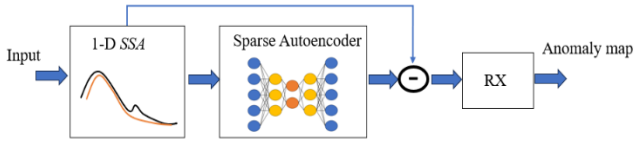

Fig.1. Architecture of the proposed method

2.1. 1-D Singular spectrum analysis (1D-*SSA*)

In the traditional classification task, the main objective of *SSA* is to extract the representative spectral information from the HSI data. For this purpose, each spectral profile will be decomposed into several independent components including trend, oscillations, or noise. Then, several components will be used to reconstruct the HSI data. In HAD task, given a hypercube $T \in \Re^{W*H*B}$, where W and H denote the size of the spatial domain, and B represents the number of spectral bands. The *SSA* algorithm will be used to reduce the noise in spectral domain corresponding to each pixel, followed by a differentiation process, as detailed below.

Let a 1-D vector $x = [x_1, x_2, \dots, x_B]$ represent a pixel randomly selected from the hypercube, it will be firstly embedded to form the trajectory matrix X by an embedding window $L \epsilon Z$ with $Z \epsilon [1, B]$.

$$X = \begin{pmatrix} x_1 & x_2 & \dots & x_K \\ x_2 & x_3 & \dots & x_{K+1} \\ \vdots & \vdots & \ddots & \vdots \\ x_L & x_{L+1} & \dots & x_B \end{pmatrix} \tag{1}$$

where $K = B - L + 1$. Each column of X is a lagged vector and can be considered as a Hankel matrix that has equal values along the antidiagonals.

Singular value decomposition (SVD) will be employed for eigen decomposition on matrix X, where the eigenvalues and eigenvectors of XX^T can be denoted as $(\lambda_1, \lambda_2, \dots, \lambda_L)$ and $(U_1, U_2, \dots, U_L)$, respectively. The trajectory matrix can be reconstructed as the sum of elementary matrices which can be represented as:

$$X = X_1 + X_i + \cdots + X_L \ (X_i = \sqrt{\lambda_i} U_i V_i^T, V_i = \frac{X^T U_i}{\sqrt{\lambda_i}}) \tag{2}$$

where the matrices U and V are denoted by the matrix of empirical orthogonal functions and the principal components after decomposition.

Divided the total set of L components into M disjoint sets $(I_1, I_2, \dots, I_M)$ where $I = [i_1, i_2, \dots, i_p]$ representing a divided set, the trajectory matrix is represented by:

$$X = X_{I1} + X_{Ii} + \cdots + X_{IM} \tag{3}$$

In order to project each divided set into a 1-D signal, let $Z_m = [Z_{m1}, Z_{m2}, \dots, Z_{mN}] \epsilon \Re^N$ denote the 1-D signal projected from X_{Im}; it can be obtained via diagonal averaging, where $\alpha_{j,n-j+1}$ refers to the elements of X_{Im}, i.e.

$$z_{mn} = \begin{cases} \frac{1}{n}\sum_{j=1}^{n} \alpha_{j,n-j+1}, & 1 \le n \le L \\ \frac{1}{L}\sum_{j=1}^{L} \alpha_{j,n-j+1}, & L \le n \le K \\ \left(\frac{1}{N-n+1}\sum_{j=n-K+1}^{L} \alpha_{j,n-j+1}, \right. & K \le n \le N \end{cases} \tag{4}$$

Finally, the original 1-D signal x can be represented using its eigenvalues in one or more principal groups, highly noisy and less significant components can be discarded, the original signal processed by SSA can be reconstructed as:

$$SSA_{(x)} = z_1 + z_2 + \cdots, + z_M = \sum_{m=1}^{M} Z_m \tag{5}$$

2.2 Sparse Autoencoder

Sparse Autoencoder is a neural network model aiming to learn efficient data representations. It minimizes the reconstruction error between input and output, incorporating sparsity by penalizing excessive neuron activations using a sparsity term. The sparsity is controlled by a sparsity proportion, adjusting the average activation. Additionally, L2 weight regularization is employed to prevent overfitting by penalizing large weights. The model is trained by optimizing the following objective function:

$$\begin{aligned} J_{(W,b)} = & \frac{1}{2m}\sum_{i=1}^{m} ||h(Wx^{(i)} + b) - x^{(i)}||^2 \\ & + \lambda \sum_{j=1}^{n} \left(\rho log^{\frac{\rho}{\hat{\rho}_j}} + (1-\rho) log^{\frac{1-\rho}{1-\hat{\rho}_j}} \right) \\ & + \frac{\beta}{2}\sum_{l=1}^{L} ||W^{(l)}||^2 \end{aligned} \tag{6}$$

where W denotes the weights, b stands for biases, $h(\cdot)$ signifies the activation function, $x^{(i)}$ represents the input, ρ indicates the sparsity proportion, λ is the sparsity weight, and β represents the L2 weight regularization strength. Here, the key parameters of the hidden size, max epochs, β, ρ and λ are set to 128, 200, 0.001, 0.001, and 0.001, respectively.

2.3 RX based anomaly map extraction

Taking the image obtained from sparse autoencoder above as the input, the RX (Reed-Xiaoli) algorithm is applied to extract the anomaly map. Specifically, RX was employed to calculate the global mean vector and covariance matrix of all the pixels within the image. For each pixel, its anomaly score can be determined by the Mahalanobis distance of its reconstruction error from the global mean and the covariance. These scores can be used to build an anomaly map, as a

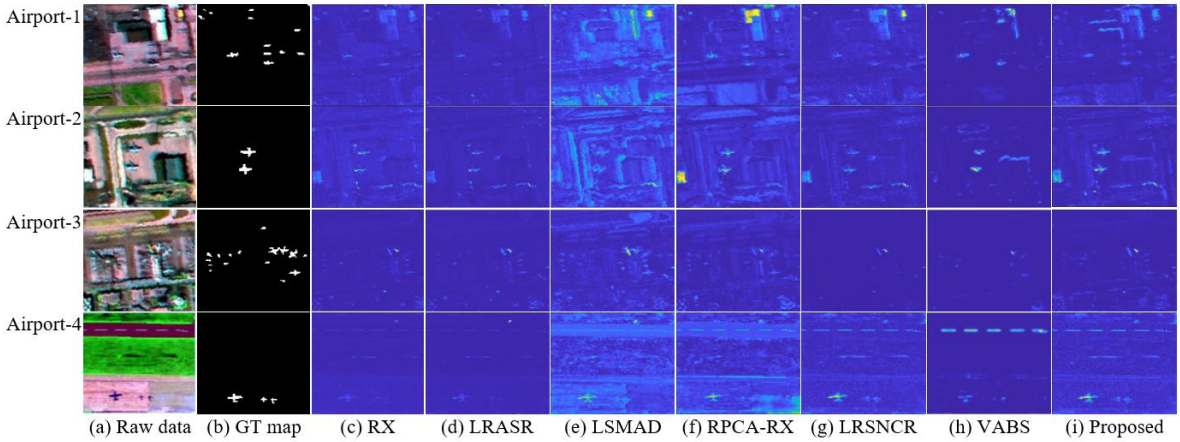

Fig. 2. Pseudo-color images (a) and corresponding ground-truth maps of four datasets and detection maps of the benchmarks, which are RX (c), LRASR (d), LSMAD (e), RPCA-RX(f), LRSNCR(g), VABS(h), proposed (i).

grayscale image, where small and large values indicate the low and high anomaly levels of the corresponding pixels, respectively. Spatial filtering can be applied for robustness.

3. EXPERIMENT RESULTS

In order to evaluate the superiority and effectiveness of our proposed method, the airport dataset comprises four images captured by the Airborne Visible/Infrared Imaging Spectrometer (AVIRIS) HSI sensor in distinct scenes were employed to test the detection accuracy. Specifically, the Airport-1, Airport-2, and Airport-3 images were acquired in Los Angeles at a spatial resolution of 7.1m, while the Airport-4 image was obtained in Gulfport with a spatial resolution of 3.4m. The pseudo-color images and corresponding ground-truth maps of the four datasets are shown in Fig. 2(a-b).

The proposed method is compared with six state-of-the-art unsupervised benchmarks including RX [3], LRASR [7], LSMAD [8], VABS [9], robust principal component analysis with RX(RPCA-RX) [10] and LRSNCR [11]. The detection intensity maps of all methods on the four datasets are shown in Fig. 2(c-i). Corresponding Area Under the Curve (AUC) values for each method on individual images, as well as the average values across all methods for the four datasets, are presented in Table 1.

First, upon visualizing the results, our proposed algorithm precisely detects anomalous aircraft targets, consistently exhibiting the highest brightness compared to other algorithms. Compared with the visual result of the original RX, due to its lack of feature extraction steps and susceptible to noise, resulted in inaccurate target identification. This confirms the significance of 1-D *SSA* and sparse AE in our proposed algorithm. Furthermore, from the quantitative analysis of the AUC values, our proposed method outperforms other benchmarks significantly for individual datasets. On average across all datasets, it outpaces the second-ranking LRSNCR by 2%. When compared to the traditional RX algorithm, it demonstrates a substantial improvement of 6.62%.

Table 1: AUC values of the different methods on the four datasets

	RX	LRASR	LSMAD	RPCA-RX	LRSNCR	VABS	Proposed
Airport-1	0.8221	0.7775	0.8317	0.8088	0.8677	0.8224	**0.9072**
Airport-2	0.8403	0.8664	0.9187	0.8426	0.9507	0.9191	**0.9725**
Airport-3	0.9288	0.8891	0.9383	0.9274	0.9526	0.9216	**0.9594**
Airport-4	0.9526	0.9846	0.9868	0.9628	0.9501	0.9331	**0.9937**
Average	0.8968	0.8729	0.9289	0.8942	0.9407	0.9176	**0.9630**

In addition, we employ separability plots to highlight the ability to distinguish anomalies from the background of each method. A box is utilized to represent data within the 20%–80% range, with a horizontal line denoting the data median. Data falling within the 0%–20% and 80%–100% ranges are depicted above and below the box, respectively, as indicated by dashed lines and beneath the box. Anomalies and background are represented by red and blue colors, respectively. Here, the method's proficiency in anomaly identification improves with the growing separation between the background and anomaly boxes.

The anomaly and background box distributions of our method and all compared ones are illustrated for each image in the airport dataset in Fig. 3 (a), where the distance between the background and anomaly boxes corresponding to our algorithm is farther than others, validating its high efficacy. Similarly, Fig. 3(b) illustrates the receiver operating characteristic curves (ROC) of different methods on the four datasets, where the position of the green curve representing our method is closest to the upper left, indicating its superior performance than other benchmarks.

4. CONCLUSION AND FUTURE WORK

In this paper, we proposed an unsupervised HAD method, which combines the 1-D SSA for feature extraction in the spectral domain, along with the sparse autoencoder for

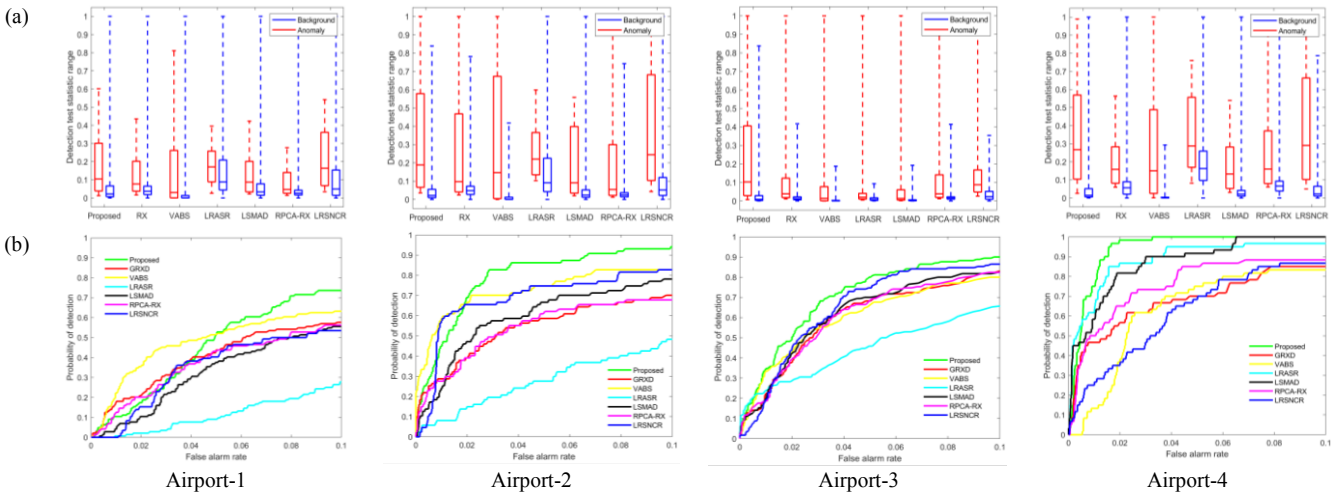

Fig. 3. Comparison of separability maps (a) and ROCs (b) of the proposed method and benchmarks on four datasets.

background reconstruction in the spatial domain, followed by the RX algorithm for identifying the anomalous pixels from the background. The experiments have validated the robustness of our method with a high detection accuracy that outperforms a few state-of-the-art HAD methods.

For future work, we plan to combine the results of noise-robust spectral reconstruction [12], semantic segmentation as well as zero-shot learning for further refined anomaly detection in an unsupervised manner, even in more generic remote sensing images rather than only HSI.

5. REFERENCES

[1] Y. Li, J. Ren, Y. Yan et al., "CBANet: An End-to-end Cross Band 2-D Attention Network for Hyperspectral Change Detection in Remote Sensing," *IEEE Trans. Geosci. Remote Sens.,* 2023.

[2] Y. Yan, J. Ren, H. Sun et al, "Nondestructive Quantitative Measurement for Precision Quality Control in Additive Manufacturing Using Hyperspectral Imagery and Machine Learning," *IEEE Tran. Industrial Inform.,* pp. 1-13, 2024.

[3] I. S. Reed and X. Yu, "Adaptive multiple-band CFAR detection of an optical pattern with unknown spectral distribution," *IEEE Trans. Acoust., Speech Signal Process.,* vol. 38, *(10),* pp. 1760-1770, 1990.

[4] H. Kwon and N. M. Nasrabadi, "Kernel RX-algorithm: A nonlinear anomaly detector for hyperspectral imagery," *IEEE Trans. Geosci. Remote Sens.,* vol. 43, *(2),* pp. 388-397, 2005.

[5] J. M. Molero, E. M. Garzon, et al., "Analysis and optimizations of global and local versions of the RX algorithm for anomaly detection in hyperspectral data," *IEEE J. Sel. Top. Appl. Earth Obs. Remote Sens.,* vol. 6, *(2),* pp. 801-814, 2013.

[6] W. Li and Q. Du, "Collaborative representation for hyperspectral anomaly detection," *IEEE Trans. Geosci. Remote Sens.,* vol. 53, *(3),* pp. 1463-1474, 2014.

[7] Y. Xu, Z. Wu, J. Li, et al., "Anomaly detection in hyperspectral images based on low-rank and sparse representation," *IEEE Trans. Geosci. Remote Sens.,* vol. 54, *(4),* pp. 1990-2000, 2015.

[8] Y. Zhang, B. Du, L. Zhang and S. Wang, "A low-rank and sparse matrix decomposition-based Mahalanobis distance method for hyperspectral anomaly detection," *IEEE Trans. Geosci. Remote Sens.,* vol. 54, *(3),* pp. 1376-1389, 2015.

[9] P. Xiang, J. Song, H. Qin, et al., "Visual attention and background subtraction with adaptive weight for hyperspectral anomaly detection," *IEEE J. Sel. Top. Appl. Earth Obs. Remote Sens.,* vol. 14, pp. 2270-2283, 2021.

[10] Y. Xu, Z. Wu, J. Chanussot et al., "Joint reconstruction and anomaly detection from compressive hyperspectral images using Mahalanobis distance-regularized tensor RPCA," *IEEE Trans. Geosci. Remote Sens.,* vol. 56, *(5),* pp. 2919-2930, 2018.

[11] W. Yao, L. Li, H. Ni, et al., "Hyperspectral anomaly detection based on improved RPCA with non-convex regularization," *Remote Sens.,* vol. 14, *(6),* pp. 1343, 2022.

[12] P. Ma, J. Ren, G. Sun, et al., "Multiscale Superpixelwise Prophet Model for Noise-Robust Feature Extraction in Hyperspectral Images," *IEEE Trans. Geosci. Remote Sens.,* vol. 61, pp. 1-12, 2023.